International Conference on Nuclear Data for Science and Technology 2007
DOI: 10.1051/ndata:07481

The cross section of the $^{16}O(n,\alpha)^{13}C$ reaction in the MeV energy range

G. Giorginis[1,a], V. Khryachkov[1,2], V. Corcalciuc[1,3], and M. Kievets[1]

[1] European Commission, Joint Research Centre, Institute for Reference Materials and Measurements (IRMM), 2440 Geel, Belgium
[2] Institute for Physics and Power Engineering (IPPE), 249020 Obninsk, Russia
[3] Institute for Physics and Nuclear Engineering, P.O. Box MG6, Bucharest, Romania

Abstract. A novel spectrometer was developed and used to measure the cross section for the $^{16}O(n,\alpha)$ reaction at IRMM. The basic parts of the new instrument are an ionisation chamber, a gas oxygen target, and signal digitisation. It is shown that simultaneous digitisation of the anode and cathode signals allows an effective background suppression and the accurate determination of the number of reaction events and the number of atoms in the gas target. Cross section values for the $^{16}O(n,\alpha)$ reaction measured in the energy range 3.95–9.0 MeV are presented. None of the existing nuclear data libraries describes well the IRMM data in the entire energy range.

1 Introduction

The $^{16}O(n,\alpha)$ cross section is of importance because oxygen is a basic constituent of many structural materials of nuclear reactors. For example in MOX fuel the reaction $^{16}O(n,\alpha)$ must be taken into account for a correct calculation of the sensitivity coefficient k_{eff}. According to the High Priority Nuclear Data Request List of the Nuclear Energy Agency a cross section uncertainty of 5% is required for $^{16}O(n,\alpha)$ in order to achieve significant improvement in applications such as reactivity predictions of thermal and fast reactors, calculation of helium production in fuel pins and claddings and calibration of neutron source strengths. This reaction is also of interest in astrophysics, dosimetry and radiobiology.

At the moment of starting the present work only limited information about the $^{16}O(n,\alpha)^{13}C$ reaction was available [1–3]. Evaluations are mainly based on measurements of the inverse $^{13}C(\alpha,n)^{16}O$ reaction [4–6]. The most recent of them, ENDF/B-VII.0, was produced from ENDF/B-VI.8 by reducing 32% the cross section values of the latter. The 32% reduction was applied in the neutron energy range 2.4–8.9 MeV although it is strictly valid from 4.2 to 6.4 MeV [6].

Our aim was to develop a new experimental method for the measurement of the $^{16}O(n,\alpha)^{13}C$ with high accuracy. The cross sections to be measured are low and the excitation function has a strong resonance structure with several resonances of width less than 100 keV. A neutron beam with a high energy resolution has to be used. This is equivalent to a low neutron flux and long measurement times at a Van de Graaff accelerator. A large number of target atoms and a spectrometer with high detection efficiency and large signal-to-background ratio can be used to measure the $^{16}O(n,\alpha)^{13}C$ cross section with a few percent accuracy in a reasonable time. This is demonstrated in the present paper.

2 Experimental method

For the detection of α particles an ionisation chamber with Frisch grid (main chamber) was used (fig. 1). The diameter of the electrodes was 18 cm, the distances cathode-to-anode and grid-to-anode were 4 cm and 3 mm, respectively. The working gas was a mixture of Kr (97%) and CO_2 (3%) at 3 bar absolute pressure. The oxygen present in the gas plays the role of the target on which the reaction (n,α) takes place. The axis of the neutron beam coincides with the symmetry axis of the chamber.

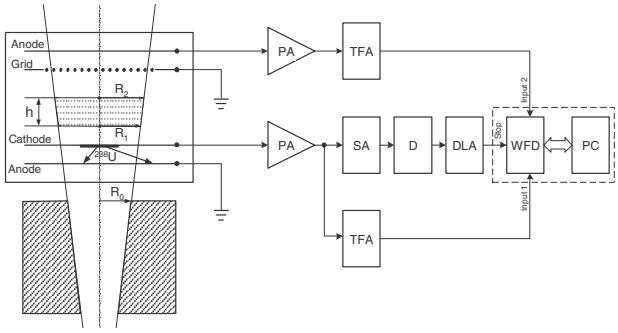

Fig. 1. Schematics of the IRMM experimental setup. PA: preamplifier, TFA: timing filter amplifier, D: discriminator, SA: spectroscopy amplifier, DLA: delay line amplifier, WFD: waveform digitizer, PC: personal computer.

A thin ^{238}U standard was used as monitor of the incident neutron beam. The fission fragments were detected by an ionization chamber which had the same cathode with the main chamber. The distance cathode-to-monitor anode was 1 mm. The common cathode signals and the anode signals of the main ionization chamber were amplified and then digitised (waveform digitiser: Signatec, model PDA12A, 12 bit, 62.5 MHz/channel). Signal digitisation was started by the data acquisition programme and was completed when a trigger signal was delivered by the cathode. The digitized signals were stored in a list mode on the hard disk of the computer for off-line analysis. The dead time of the spectrometer is identical for charged particles detected in the main chamber and fission fragments detected in the monitor chamber, because signals of both particles are fed to the same electronic (cathode) channel.

[a] Presenting author, e-mail: georgios.giorginis@ec.europa.eu

3 Data processing

The spectrometer provides two types of signals (fig. 2): i) an anode and a cathode signals from the main chamber; ii) a cathode signal from the monitor chamber. The data acquisition system digitises and stores these signals as anode and cathode signals without discrimination between the two different cathode signals. The first step of the off-line analysis is separation of the two signal types i) and ii). By demanding nonzero amplitudes for anode and cathode only signals of type i) are selected. For nonzero cathode and zero anode amplitudes, respectively only signals of type ii) are obtained. Additionally a pulse amplitude spectrum for type ii) signals is produced. It is used to determine the number of the incident neutrons.

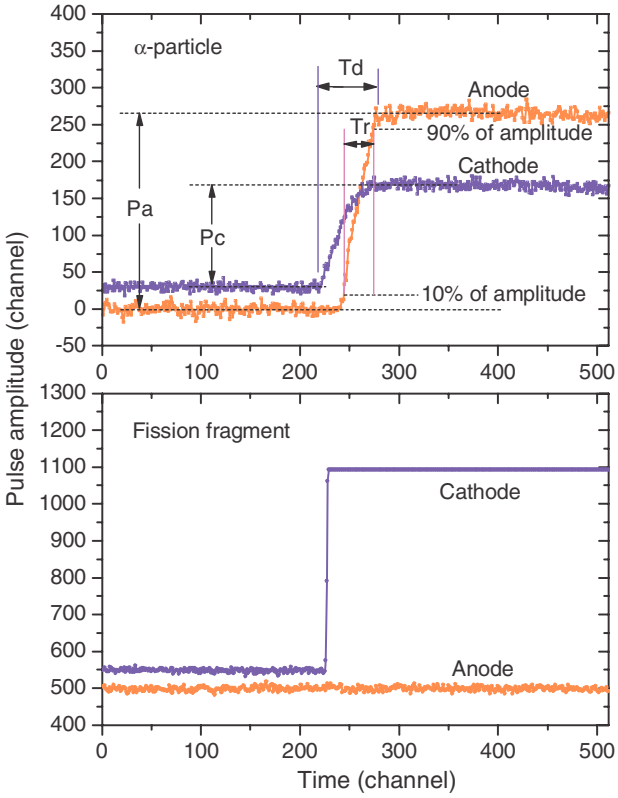

Fig. 2. Digitized signals of the main chamber and of the neutron monitor chamber.

The signals of type i) are subject to a more complicated analysis. From them, the following information is extracted: amplitude of the anode (P_A) and cathode (P_C) signals, time of origin of the anode (T_{SA}) and cathode (T_{SC}) signals and the time the anode signal reaches its maximum (saturation) (T_{EA}). The latter corresponds to the time of the completion of charge collection at the anode. The basic parameters used in the analysis are: the amplitudes of the signals, the drift time of the origin (or end) of the particle track $T_D = (T_{EA}–T_{SC})$ and the rise time of the anode signal $T_R = (T_{EA}–T_{SA})$. As is shown in section 4 the drift time can be converted to the distance covered by the origin (or end) of the particle track as it moves along the direction of the neutron beam. The rise time corresponds to the time spent by the projection of the particle

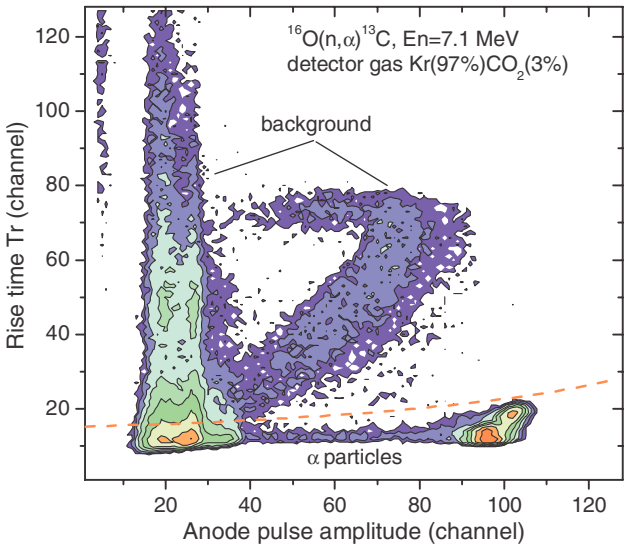

Fig. 3. Two-dimensional spectrum of rise time versus amplitude of anode pulse with the dashed line separating a particles from background.

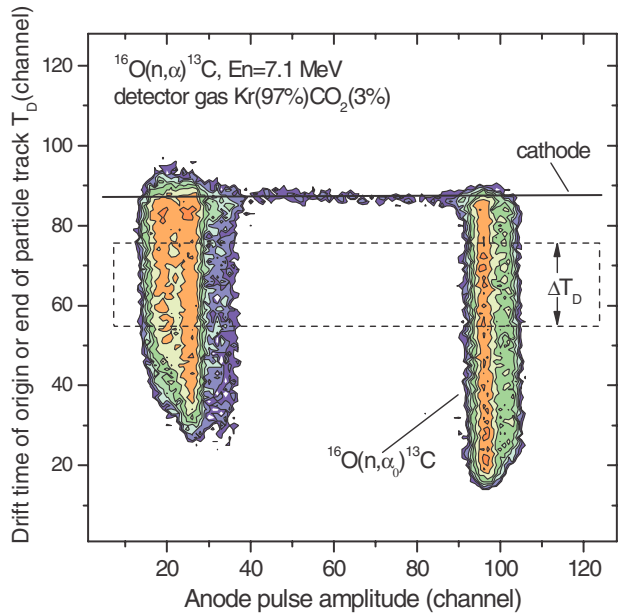

Fig. 4. Two-dimensional spectrum of drift time versus the anode pulse amplitude. The dashed rectangle defining the region of interest for the analysis. The drift time window ΔT_D determines the height of the effective volume of the gaseous target $\Delta x = h$.

track to pass the grid-to-cathode distance. Measurement of the rise time is equivalent to the determination of the projection of the particle track on the neutron beam direction. From this comes the name time projection chamber (TPC) of the spectrometer. Figure 3 shows the two-dimensional spectrum of the rise time versus anode pulse amplitude. It provides a clean separation between signals from ^{16}O(n,α_0) and background reactions on the electrodes and detector gas [(n,p), (n,α), (n,recoil)].

The two-dimensional spectrum of the drift time versus anode pulse amplitude for the events below the dashed line

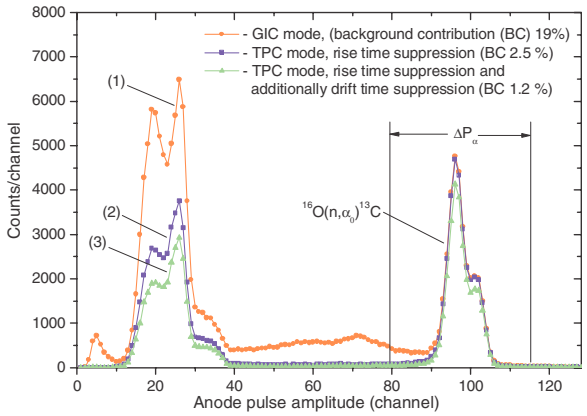

Fig. 5. Pulse amplitude spectrum: (1) GIC mode, (2) after rise time suppression of background, (3) after rise time and drift time suppression of background. The percentages in brackets show the background contribution to the α particle line.

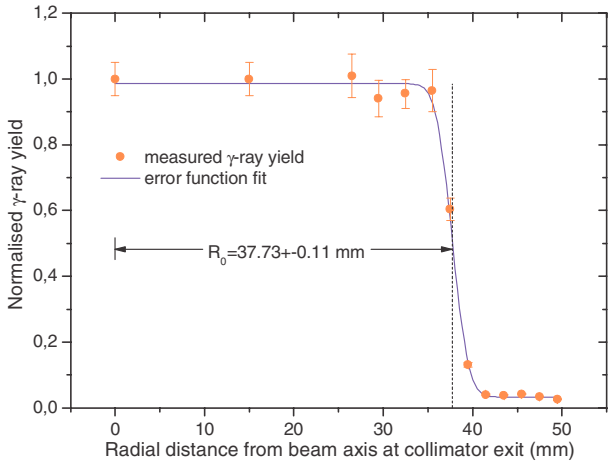

Fig. 6. Fast neutron beam profile at the exit of a Cu collimator.

in figure 3 is shown in figure 4. The drift time window ΔT_D determines the height of the effective volume of the gas target $\Delta x = h$ as is shown below. The definition of the latter is that only those α particles from $^{16}O(n,\alpha_0)$ are selected, which are fully stopped in the detector gas without to touch the electrodes. The application of the window ΔT_D further suppresses background originating at the electrodes.

The pulse amplitude spectra of the anode shown in figure 5 are a comparison for background suppression between a conventional gridded ionisation chamber (GIC) and the TPC spectrometer. A 99% background suppression was achieved by our TPC compared with the 80% value of a conventional GIC. The pulse amplitude window ΔP_α is used to determine the number of $^{16}O(n,\alpha_0)^{13}C$ events.

4 Number of atoms in the gas target

Particular attention was devoted to the determination of the effective volume of the gas target, from which the number of the oxygen atoms is obtained. A rotational symmetric copper collimator was used to obtain a conical neutron beam, so that the shape of the gas target is a truncated cone (fig. 1). The precise values of the radii of the two basis surfaces R_1 and R_2, are mandatory for an accurate determination of the volume of the working gas. For the measurement of the neutron beam profile the activation method with threshold reactions on Al and In at neutron energies of 7.4 and 2.5 MeV, respectively, was used. As example, the measured beam profile at the exit of the collimator for 7.4 MeV neutron energy is shown in figure 6. The radii R_1 and R_2 were obtained from the beam radius R_0 at the collimator exit.

This novel method of fast neutron beam profiling allows to determine the diameter of the neutron beam with an uncertainty of 0.1 mm (fig. 6). Knowing the volume, temperature, pressure, and the composition of the gas target the number of oxygen atoms was determined by using the equation of ideal gases.

The height of the gas target is deduced from the distribution of the drift time T_D which is limited between a minimum and a maximum value T_A and $T_C + T_A$, respectively. T_A is the drift time between grid and anode for charged particles created very close to the grid and their tracks are parallel to it. T_C is the drift time between cathode and grid for charged particles created very close to the cathode and their tracks are parallel to it. The ionisation electrons move between cathode and grid with a constant drift velocity $v_e = D/T_C$, where D is the distance from cathode to grid. T_C was obtained from the T_D distribution with an uncertainty of 1%. The drift time distribution is converted to a position distribution for the origin (or end) of particle tracks between cathode and grid by applying the linear relation $x = v_e T_D = (D/T_C)T_D$. The height of the gas target is $\Delta x = h = (D/T_C)\Delta T_D$, where ΔT_D is a suitable drift time window as specified above.

5 Neutron flux

For the production of monoenergetic neutrons below 4.4 MeV the $T(p,n)^3He$ reaction on a 214 $\mu g/cm^2$ thick solid TiT target with a silver backing was used. Above 4.96 MeV the neutron source was the $D(d,n)^3He$ reaction on a gaseous deuterium target with a 5 μm molybdenum entrance window and a tantalum plate as stop of the deuteron beam. The deuteron pressure was 20 and 50 kPa for neutron energies below and above 7.4 MeV, respectively. The width of the energy distribution for the p-T reaction varied from 14 to 13 keV for neutron energies between 3.95 and 4.35 MeV, respectively. For the d-D reaction it varied, in terms of energy loss of the deuteron beam in the deuteron gas, from 52 keV to 21 keV for neutron energies from 4.96 to 9.0 MeV, respectively. Inhomogeneities of the molybdenum foil produced a dominating contribution between 157 and 86 keV.

A ^{238}U standard of 549 $\mu g/cm^2$ thickness and a 2.54 cm diameter mounted on the common cathode in a back-to-back geometry relative to the main chamber assured the accurate monitoring of the neutron flux. The background of neutrons produced by the incident charged particles on the backings or entrance window was measured by using a Ti/Ag blank for $T(p,n)^3He$ and the gas deuterium target evacuated for $D(d,n)^3He$. The effect of scattered neutrons in the collimator and on the walls of the experimental hall was determined as well by performing measurements with open and closed collimator under identical conditions.

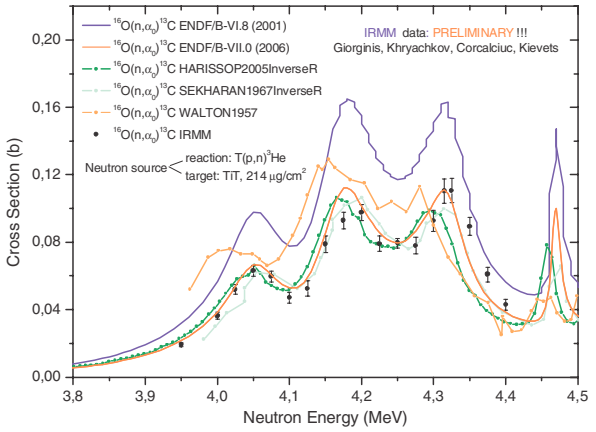

Fig. 7. Cross section of ^{16}O(n,α_0)^{13}C measured at IRMM between 3.95 and 4.4 MeV in comparison with ENDF evaluations and other data obtained from measurements of ^{16}O(n,α_0)^{13}C and the inverse reaction ^{13}C(α,n)^{16}O.

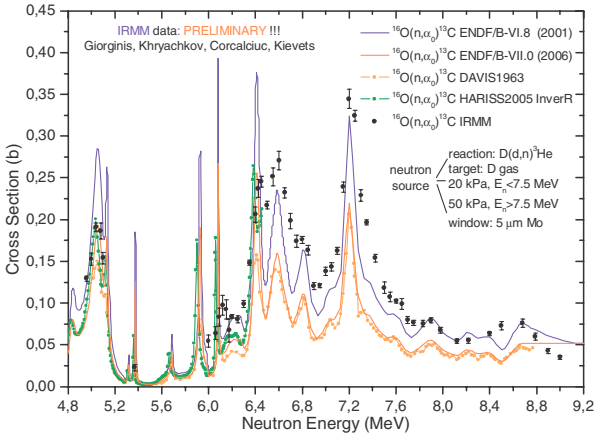

Fig. 8. Cross section of ^{16}O(n,α_0)^{13}C measured at IRMM between 4.96 and 9 MeV in comparison with ENDF evaluations and other data obtained from measurements of ^{16}O(n,α_0)^{13}C and the inverse reaction ^{13}C(a,n)^{16}O.

6 Uncertainties

The uncertainty of the cross section is composed mainly of contributions from the following sources of uncertainty: a) number of oxygen nuclei in the gaseous target and b) number of reaction and monitor events. Contribution a) consists of uncertainties of the: 1) radii of the surfaces of the truncated cone (0.1 mm or 1.1%), 2) height of the gas volume (1%), 3) pressure of the detector gas (0.1%), 4) temperature of the detector gas (0.3%), and 5) content of CO_2 (2%) as certified by the producer. Finally, the overall uncertainty in the number of oxygen-16 nuclei amounts to about 2.5%.

Contribution b) consists of uncertainties arising from: 1) counting statistics of reaction and monitor events (<5% for the majority of the measurement points from 3.95 to 9 MeV), 2) background suppression (1.2%), 3) correction for neutron background from structural materials of the neutron sources (1.5%), 4) the uncertainty of the number of ^{238}U nuclei in the monitor sample (<0.7%), and 5) the determination of low energy monitor events by extrapolation (<1.5%).

The total systematic uncertainty obtained by quadratic addition of the individual contributions of a) 2.5% and b) 3.6% amounts to 4.4%. Combining this with the statistical uncertainty of about 5% an overall cross section accuracy of 6.6% is obtained.

7 Results and discussion

A novel spectrometer with signal digitisation and gas reaction target was developed and used to measure the cross section for the ^{16}O(n,α) reaction at IRMM. There are a series of advantages by using an ionisation chamber with signal digitisation and a gaseous target, wherever applicable. The experimental setup is simple because a minimum of electronic modules is used. Energy, track origin, and identification of the detected particles are obtained from the amplitude and time information contained in the digitised pulses. An effective background suppression and a high signal-to-noise ratio can be achieved. Gaseous targets are superior to solid samples for several reasons: 1) the number of nuclei in the effective gas volume is about 100 times larger than the one in a solid target used for similar measurements, 2) the number of target nuclei can be determined with high accuracy with simple methods, 3) the energy spectrum obtained with gaseous targets is very simple because the energy of both reaction products, which is equal to the neutron energy plus the Q-value of the reaction. Furthermore energy losses, which are a problem in the case of solid targets especially at large emission angles, do not exist for gaseous targets.

Cross section values for ^{16}O(n,α_0)^{13}C were determined by using an equation relating measured reaction and monitor yields with the corresponding cross sections, number of atoms, and the geometry of the gas target. Results are shown in figure 7 and figure 8 for neutron energies from 3.9 to 4.4 MeV and from 4.96 to 9 MeV, respectively. Data of other experiments for ^{16}O(n,α_0)^{13}C, data obtained from measurements of the inverse ^{13}C(α,n)^{16}O reaction, and evaluated cross sections from ENDF/B-VI.8 and ENDF/B-VII.0 are also shown for comparison.

Below 6.4 MeV the IRMM measurements so far are in good agreement with ENDF/B-VII.0 and the Harissopulos et al. [6] measurement of the inverse reaction ^{13}C(α,n)^{16}O. Above 6.4 MeV the IRMM data are close to the values of ENDF/B-VI.8, but there is disagreement with ENDF/B-VII.0.

References

1. J. Seitz et al., Helv. Phys. Acta **28**, 227 (1955).
2. R.B. Walton et al., Phys. Rev. **107**, 1065 (1957).
3. E.A. Davis et al., Nucl. Phys. **48**, 169 (1963).
4. K.K. Sekharan et al., Phys. Rev. **156**, 1187 (1967).
5. J.K. Bair et al., Phys. Rev. C **7**, 1356 (1973).
6. S. Harissopulos et al., Phys. Rev. C **72**, 062801(R) (2005).